ACS APPLIED MATERIALS & INTERFACES

Research Article

www.acsami.org

Strong and Electrically Conductive Graphene-Based Composite Fibers and Laminates

Ivan Vlassiouk,*[,†] Georgios Polizos,[†] Ryan Cooper,[†] Ilia Ivanov,[†] Jong Kahk Keum,[†] Felix Paulauskas,[†] Panos Datskos,[†] and Sergei Smirnov[‡]

[†]Oak Ridge National Laboratory, Oak Ridge, Tennessee 37830, United States

[‡]Department of Chemistry and Biochemistry, New Mexico State University, Las Cruces, New Mexico 88011, United States

Supporting Information

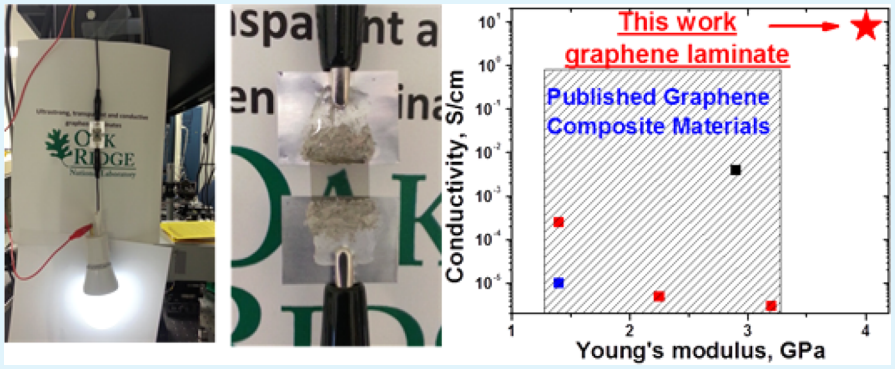

ABSTRACT: Graphene is an ideal candidate for lightweight, high-strength composite materials given its superior mechanical properties (specific strength of 130 GPa and stiffness of 1 TPa). To date, easily scalable graphene-like materials in a form of separated flakes (exfoliated graphene, graphene oxide, and reduced graphene oxide) have been investigated as candidates for large-scale applications such as material reinforcement. These graphene-like materials do not fully exhibit all the capabilities of graphene in composite materials. In the current study, we show that macro (2 inch × 2 inch) graphene laminates and fibers can be produced using large continuous sheets of single-layer graphene grown by chemical vapor deposition. The resulting composite structures have potential to outperform the current state-of-the-art composite materials in both mechanical properties and electrical conductivities (>8 S/cm with only 0.13% volumetric graphene loading and 5×10^3 S/cm for pure graphene fibers) with estimated graphene contributions of >10 GPa in strength and 1 TPa in stiffness.

KEYWORDS: *graphene, mechanical properties, composites, strength, chemical vapor deposition*

Carbon materials are very attractive for lightweight strong materials because of stiff and high-strength sp^2 and sp^3 C−C bonds combined with low densities of carbon allotropes. Recently, graphene was proposed as an ideal candidate for lightweight, high-strength composite materials given its superior mechanical properties (specific strength of 130 GPa and stiffness of 1 TPa).[1] To date, easily scalable graphene-like materials in a form of separated flakes (exfoliated graphene, graphene oxide, and reduced graphene oxide) have been investigated as candidates for large-scale applications such as material reinforcement.[2−11] Composites employing exfoliated graphene-like materials as fillers enjoy a strong foundation of polymer nanocomposites, which has been built by decades of intensive research.[12,13] In recent years, macro samples of various carbon materials have been produced and tested. For example, yarns/ropes were prepared from carbon nanotubes (CNT)[14−16] and various types of graphene-like materials.[17−19] Performance of such materials was shown to be very promising, but the demonstrated mechanical properties were still below those of high-quality carbon fibers. Weak bonding between small graphene sheets (or CNTs) leads to poor load transfer. Eliminating these weak links or using larger scale graphene should result in better quality lightweight and electrically conductive materials with mechanical properties approaching those of individual graphene crystals measured at the micro level.

Composite materials using various polymer matrices with graphene and graphene oxide flakes as reinforcement elements were described in literature, but the fillers either had a tendency to agglomerate, which results in poor dispersion in the matrix (in the case of graphene), or had inferior mechanical properties because of introduced structural modifications (in the case of graphene oxide).[2−8] The small size of graphene sheets and poor control over the number of graphene layers in exfoliated samples also causes poor load transfer with polymer matrix and limited electrical conductivity.

Received: December 5, 2014
Accepted: April 28, 2015
Published: April 28, 2015

DOI: 10.1021/acsami.5b01367
ACS Appl. Mater. Interfaces 2015, 7, 10702−10709

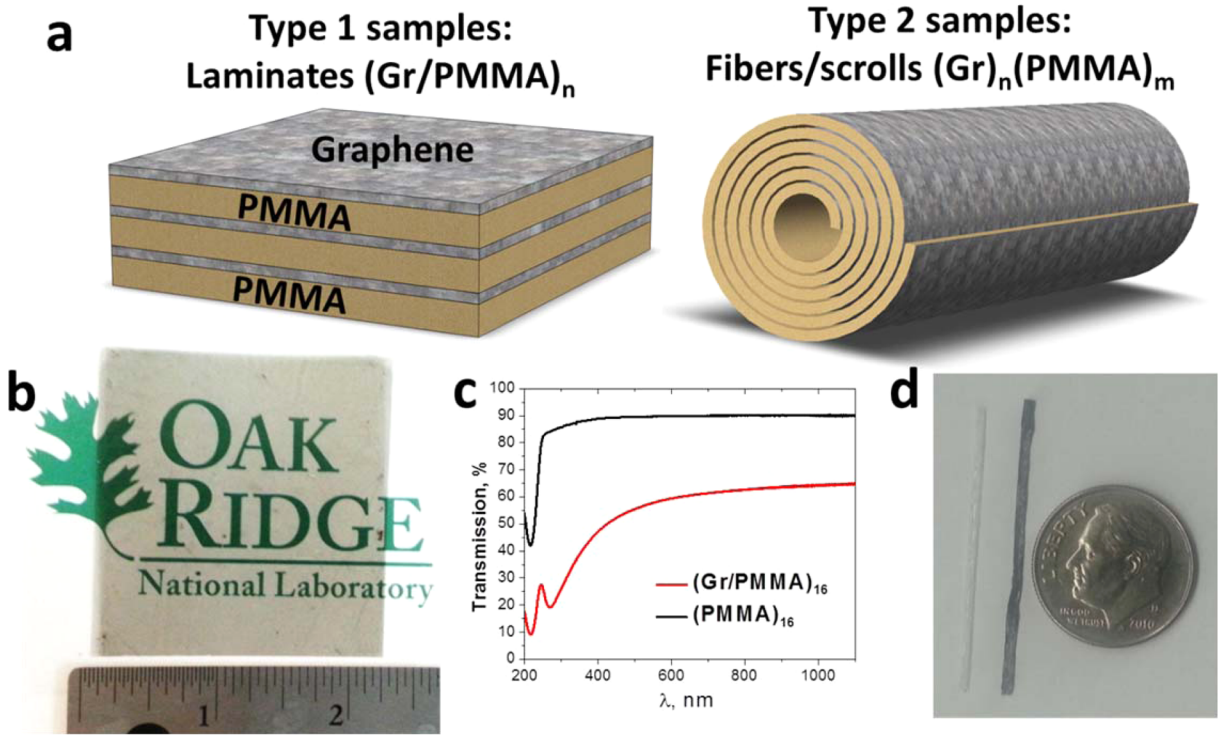

Figure 1. Description of type-1 and -2 samples used in this work. (a) Scheme of laminates and fibers/scrolls. (b) $(Gr/PMMA)_{16}$ laminate. (c) UV/vis spectra of $(Gr/PMMA)_{16}$ and $(PMMA)_{16}$ laminates. (d) Photograph of $(PMMA)_1$ fiber (left) and $(Gr)_6/(PMMA)_1$ fiber (right).

Graphene grown via chemical vapor deposition (CVD graphene) can solve several of the aforementioned fundamental problems typical for exfoliated graphene-like materials by offering (a) large lateral size of continuous graphene and thus efficient load transfer from matrix, (b) uniform and controllable dispersion in the polymer matrix, and (c) controllable electrical and thermal conductivities. In addition, potentially cost-effective roll-to-roll production of 2D CVD graphene could create the opportunity to construct composite structures that were previously not possible with other carbon additives such as CNTs or carbon black.

RESULTS AND DISCUSSION

Graphene was grown by atmospheric pressure chemical vapor deposition on Cu foils as described earlier.[20,21] Our graphene samples are almost exclusively single-layer (<5% of bilayer coverage) with a polycrystalline structure where the average size of domains (grains) exceeded 100 μm. The final defect concentration inside the graphene domain was below the detection limit of Raman spectroscopy (<1 defect per 0.25 μm^2). In this work, we prepared two different types of graphene samples, which are illustrated in Figure 1a.

Type-1 samples are flat graphene laminates layered with poly(methyl methacrylate) (PMMA) matrix. This geometry is similar to copper/graphene laminates prepared on a much smaller scale[22] and to the layer-by-layer assembly approach used previously for clay and carbon nanotube laminates.[23−25] We will refer to these samples as $(Gr/PMMA)_n$ with n identifying the number of consecutive Gr/PMMA layers that were transferred one at the time with annealing upon transferring of an additional Gr/PMMA layer onto the laminate (Methods).

Type-2 samples are scrolls of laminates, and we will refer to them as fibers. These fibers were prepared by rolling up the layered structures on a wire with 0.7 mm diameter. For example, a $(Gr)_1/(PMMA)_1$ sample was prepared by rolling up a laminate consisting of a single graphene layer on top of a single PMMA layer into the fiber, whereas $(Gr)_6/(PMMA)_1$ has six graphene layers on top of a single PMMA layer rolled up into fiber. In every sample described above, individual PMMA layer thickness was approximately 250 nm, as prepared by spin coating. Finally, we have prepared pure graphene fibers and denote them as $(Gr)_6$, where the subscript identifies the number of graphene layers in the fiber. It was produced by dissolving PMMA from a $(Gr)_6/(PMMA)_1$ fiber.

Typical samples are presented in Figure 1. Figure 1b shows a 2 inch square sample of $(Gr/PMMA)_{16}$, which results in the UV/vis spectrum given in Figure 1c (red line). The 270 nm absorption peak is due to graphene (red line), whereas the peak at 215 nm comes from PMMA, as illustrated by comparison with $(PMMA)_{16}$ sample in the same graph (black line). $(PMMA)_{16}$ reflects about 10% of incident light in the visible range, as seen in Figure 1c, and a greater optical density for $(Gr/PMMA)_{16}$ comes from absorption by graphene. Single-layer graphene absorbs about 2.3% of visible light; thus, 16 layers should have optical transmission equal to $\sim 0.69 = (0.977)^{16}$, which is close to that observed in Figure 1c. Figure 1d shows a second type of samples: a $(PMMA)_1$ fiber (left) and a $(Gr)_6(PMMA)_1$ fiber (right). The pure PMMA fiber is translucent, whereas the fiber with graphene has distinct black color. The wire diameter used for fiber preparation was 0.7 mm, and because the original sample length was approximately 51 mm, the total number of layers in all samples of the second type is close to 23. The sample shown in Figure 1d had six graphene layers before it was rolled up; hence, the total number of graphene layers is close 140 with only 4% of light transmission, making it essentially black.

DOI: 10.1021/acsami.5b01367
ACS Appl. Mater. Interfaces 2015, 7, 10702−10709

Type-1 Samples. Samples similar to those shown in Figure 1b were cut into ~5 × 10 mm^2 strips and mounted on either a microtensile setup designed for mesoscale testing or a commercially available setup (Supporting Information and Figure 2a) to obtain the stress–strain curves. Stresses were

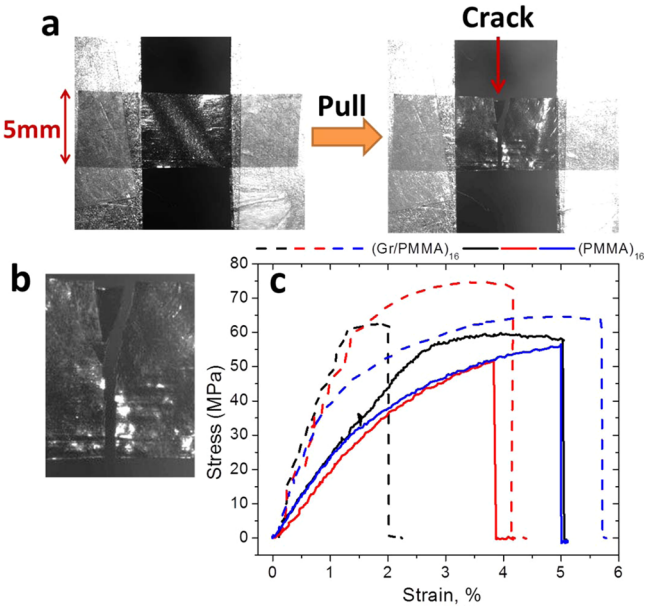

Figure 2. Strain–stress curves for type-1 samples. (a) Photograph of a $(Gr/PMMA)_{16}$ sample mounted onto holders with double-sided Scotch tape for strain–stress curves measurements; width is 5 mm. (b) Zoomed-in image of a crack developed after sample breakage. (c) Stress–strain data. Solid lines, $(PMMA)_{16}$ samples; dashed lines, $(Gr/PMMA)_{16}$ samples.

calculated by dividing the applied force by the laminate cross-sectional area. The laminate thickness was measured on a profilometer (Supporting Information). Typical stress–strain curves for laminates without graphene, i.e., $(PMMA)_{16}$, are shown as solid lines in Figure 2c. The Young's modulus, E_{PMMA} = 2.5 ± 0.4 GPa, and tensile strength, σ_{PMMA} = 53 ± 4 MPa, obtained as a result, fall within the published values for PMMA. Incorporation of graphene monolayer between each PMMA layer in the $(Gr/PMMA)_{16}$ sample resulted in a significant improvement for both the strength and the modulus. The stress–strain curves for such hybrid laminates are shown as dashed lines in Figure 2c and correspond to the modulus of E_E = 4 ± 0.5 GPa and strength of σ_E = 67.1 ± 7.5 MPa. Thus, addition of only 0.13% (by volume) of CVD graphene almost doubled the modulus and increased the strength by 25% as compared to the values of neat PMMA. Using a simple rule of mixtures, one can estimate the effective graphene mechanical properties in such composite by using the equations

$$\sigma_E = \sigma_{PMMA} V_{PMMA} + \sigma_{Gr} V_{Gr}$$

and

$$E_E = E_{PMMA} V_{PMMA} + E_{Gr} V_{Gr}$$

where σ stands for the tensile strength, E stands for modulus, V stands for volume fraction ($V_{PMMA} + V_{Gr} = 1$), and the subscripts denote pure PMMA (PMMA), pure graphene (Gr), and graphene/PMMA laminate (E). Because the volume fraction of graphene in the laminate is small, $V_{Gr} \approx (1.3 \pm 0.2)10^{-3}$ or 0.13%, and the rule of mixtures does not necessarily represent the best description, the contributions of graphene can be only viewed as estimates, giving σ_{Gr} = 11 ± 6.7 GPa and E_{Gr} = 1.2 ± 0.5 TPa, respectively. Note that graphene strength here is rather on the low limit because the rule of mixtures is less accurate for small volume fractions of filler (Supporting Information). The lower bound of the graphene modulus falls close to the recently measured modulus for CVD graphene in PEMA/graphene sandwiches.[26] When compared with small single-crystal graphene samples,[1] the effective graphene strength in our samples is an order of magnitude lower, but the modulus is surprisingly ca. 20% greater, which can be attributed to the possible orientation of the polymer chains on the graphene/PMMA interface as discussed below.

The reduction of tensile strength in our macro samples of polycrystalline graphene is not surprising, and several reasons can be identified. First, the polycrystalline nature of graphene with grain boundaries between individual domains is known to significantly reduce its strength. A few reported experimental and theoretical estimates of this effect suggest an approximately threefold reduction of the value.[27−30] Second, large-scale graphene always has defects such as vacancies that contribute to further strength degradation.[31] Raman analysis of our samples suggests that the defect densities are extremely low, at a level that should not significantly affect the samples strength. Nevertheless, for the samples of such "macro" size, it is impossible to guarantee that there are not a few large defects at random locations that could create weak points. Third, the transfer procedure during sample assembling may introduce ruptures and tears in graphene, which would have the highest effect on the strength of large-scale graphene samples.[32] These micro- and nanoscale defects can affect the graphene strength but should not significantly alter the measured modulus values.

Some papers report values for Young's modulus for single-crystal graphene higher than 1 TPa, for example, 2 TPa was estimated by Raman spectroscopy,[33] but the most widely accepted is the 1 TPa value.[1,39] The effective stiffness of graphene in our samples is 20% higher than that measured on pure single-crystal graphene (1.2 TPa or higher vs 1 TPa). The effect is within the error of the estimated effective modulus for graphene in our laminates, but it can be rationalized because of additional stiffness induced in the polymer by interaction with graphene. PMMA chains do not experience confinement effects,[34−36] as was confirmed by 2D GIWAXS (Supporting Information). Indeed, the radius of gyration (R_G ~ 25 nm) of 495 kDa PMMA used in our laminates is an order of magnitude less than the thickness of PMMA layer (250 nm) sandwiched between the two graphene layers. However, PMMA chains in proximity of the graphene surface (< R_G) are more oriented by graphene, thus effectively appear to have a larger stiffness value. Differential scanning calorimetry showed that (Supporting Information) the glass transition temperature of PMMA in $(Gr/PMMA)_{16}$ laminates was 3° lower than for pure $(PMMA)_{16}$, suggesting a weaker interaction between PMMA and graphene as compared to the interaction between PMMA globules. This indicates that the effect of increasing stiffness is due not to efficient load transfer between graphene and PMMA but more likely to polymer orientation at the interface.

Raman spectroscopy allows monitoring stress in $(Gr/PMMA)_{16}$ laminates and the effect of phonons softening under applied strain, which is well-characterized for a variety of carbon materials.[37] Several groups have reported redshifts in the Raman spectra under strain for graphene prepared by mechanical exfoliation. The reported redshift for G and 2D

DOI: 10.1021/acsami.5b01367
ACS Appl. Mater. Interfaces 2015, 7, 10702−10709

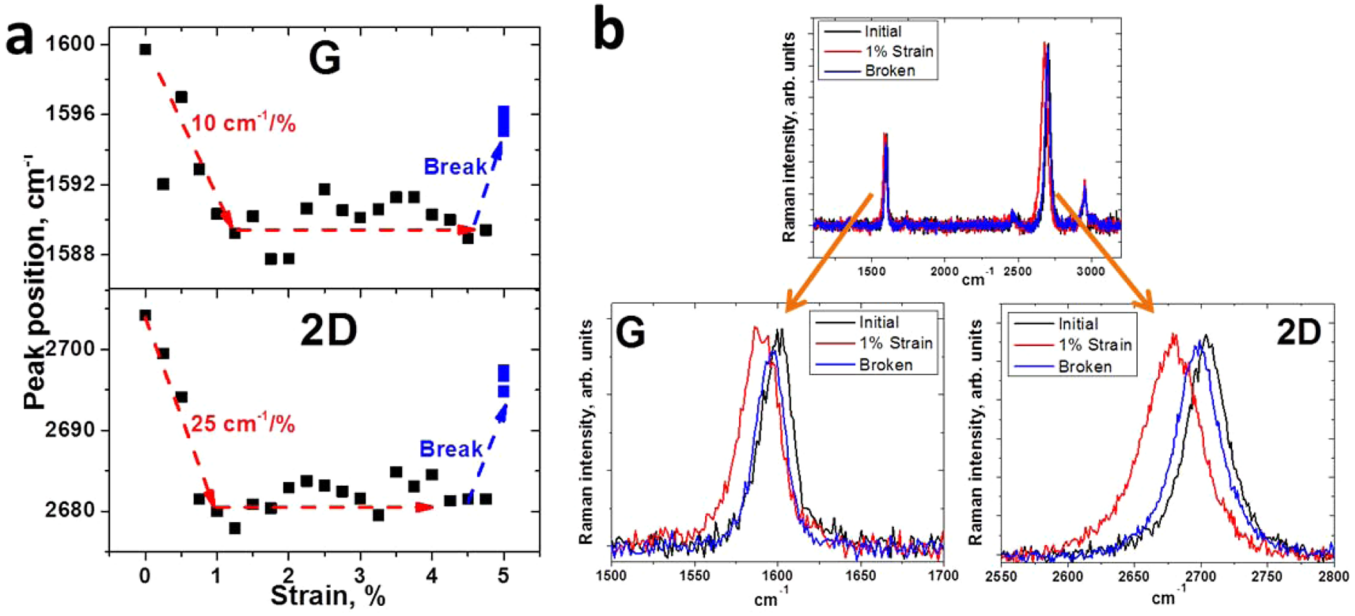

Figure 3. Shift of Raman bands vs applied strain for a $(Gr/PMMA)_{16}$ sample. (a) 2D and G bands shift and (b) Raman spectra: initial, black; 1% strain, redl and broken sample, blue.

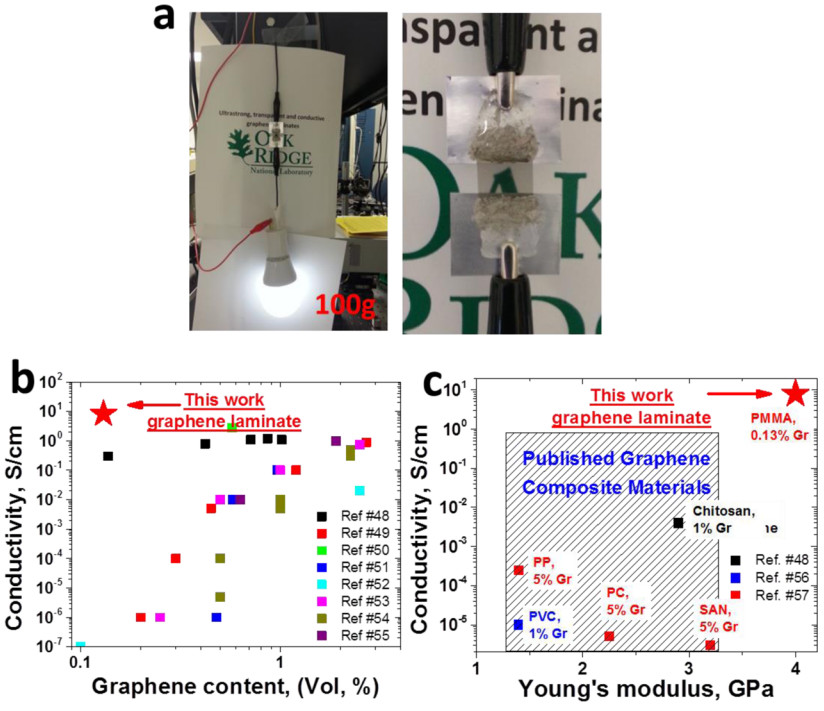

Figure 4. (a) LED lamp weighing 100 g suspended on the transparent and electrically conductive $(Gr/PMMA)_{16}$ laminate. (b) Conductivity vs graphene content chart for different polymers and graphene preparation methods (Supporting Information). (c) Conductivity vs modulus chart. In b and c, results of this work are shown as red stars.

bands varied dramatically.[38−41] For example, the 2D line varied from 7.8 cm^{-1}/% (percent of strain)[38] to more than 60 cm^{-1}/% in ref 39. In the latter paper, the G line further splits into a G^+/G^- doublet with anisotropic behavior with respect to orientations of strain and light polarization. Figure 3 shows Raman shifts for both G and 2D lines versus applied strain for the $(Gr/PMMA)_{16}$ sample. Note that the D line intensity is almost undetectable, which indicates the high quality of our graphene. The redshifts have apparent linear regions for strains up to 1% with ∼25 cm^{-1}/% for 2D and ∼10 cm^{-1}/% for G lines, respectively. These shifts are less than half of the maximum ones reported for single-crystal small exfoliated flakes.[39] Notably, the maximum strain for linear response is ∼1%, similar to those for single-crystal flakes. Upon further strain increase, the positions of the Raman bands remained unchanged until the breakage of the sample at ∼5%. After that, the peaks' positions recover but incompletely. The depth of field for our Raman setup is larger than the sample thickness, 6 μm versus 4.1 μm; thus, we get the averaged signal from all 16 graphene layers that have random crystallographic orientations

DOI: 10.1021/acsami.5b01367
ACS Appl. Mater. Interfaces 2015, 7, 10702−10709

to the laser excitation polarization that was parallel to the applied strain. We did not observe any noticeable G band splitting, but both G and especially 2D bands were broadened indicating nonuniform stress among the layers, making it hard to estimate the Young modulus from the Raman shifts for our geometry.[19,39] Smaller Raman band shifts also indicate nonuniform stress distribution, potential interface slippage, as reported earlier for much smaller sample sizes,[2,42,43] and possible graphene wrinkles.[44,45] Nevertheless, Raman spectra taken at different positions across the sample were almost identical, pointing to a rather uniform stress distribution across the sample's plane.

Type-2 Samples. $(Gr)_1(PMMA)_1$ graphene fibers demonstrated similar improvements in the strength compared to bare $(PMMA)_1$ fibers, giving an estimated graphene strength of 19 ± 9 GPa (Supporting Information). The scroll-like structure (Figure 1a) of the samples allowed for the layers sliding against each other, which would result in a greater variation of the measured modulus, thus making it harder to reliably estimate the contribution of graphene to the modulus in the produced fibers. Notably, $(Gr)_1(PMMA)_1$ samples had much better reproducibility in stress−strain curves compared to $(PMMA)_1$ fibers.

The fibers which involved a PMMA dissolution step, such as $(Gr)_6(PMMA)_1$ and $(Gr)_6$ samples, showed slightly lower strength, 2.2−4 GPa, but this is still higher than most of those reported for CNTs and graphene yarns that did not exceed 2.1 GPa.[16,18] The modulus for $(Gr)_6$ fiber was measured up to 0.3 TPa (the highest value), which is also less than the effective modulus of graphene in the laminate structures but higher than that of other carbon materials, such as graphene and CNT papers/yarns. We attribute the lower values for the fibers without PMMA to solvent trapped between graphene layers (Supporting Information) and possible ruptures of graphene by surface tension during PMMA dissolution and solvent drying.

To demonstrate the outstanding properties of produced composite materials, we suspended a commercially available LED with a mass of approximately 100 g on the transparent and flexible graphene laminates as well as on fibers (Figure 4a). Electrical conductivity of these samples was determined to be 8.1 S/cm (Supporting Information), which is higher than that reported for various graphene composites (Figure 4b,c). Pure graphene fibers have a conductivity of 5×10^3 S/cm (Supporting Information), which is similar to the values measured earlier for CNT yarns.[46,47] We did not observe a decrease in conductivity with samples bending or aging.

Figure 4b shows a conductivity/graphene content chart for different polymers and graphene preparation methods along with the results of this work. Reported percolation thresholds for composites to become electrically conductive varies, but is usually around 0.5% (volumetric).[48−55] Our proposed laminates have the highest conductivity reported so far (8.1 S/cm), with the lowest graphene volume loading percentage, 0.13%. Such high electrical conductivities were never reached using graphene-like flake fillers, even with more than 2 orders of magnitude higher loadings. Figure 4c shows conductivity/modulus plot for various polymers and graphene preparation techniques. The reported values in this work fall among the highest reported in the literature.

CONCLUSIONS

We produced macro-scale polymer/graphene laminates and fibers as well as pure graphene fibers that demonstrate the use of graphene as a reinforcing material for production of strong, flexible, transparent, and electrically conductive composite materials. We have shown that large scale CVD graphene is superior to previously employed carbon additives such as CNTs, carbon fibers, and graphene-like materials used in production of yarns, mats, and fibers, especially when it comes to producing strong conductive composites. Single-layer graphene produced by CVD allows for the circumvention of problems accompanying exfoliated graphene materials, such as difficulties with dispersion and small size flakes of poorly controlled thickness, which require high filler loadings for decent electrical and thermal conductivities. The strength of graphene/PMMA laminates is double of that for PMMA with only a 0.13% load of graphene corresponding to the effective strength of graphene in excess of 10 GPa. The effective contribution of graphene to stiffness in laminates is greater than 1 TPa, which exceeds that of monocrystalline graphene and is in part due to the orientation of polymer near the graphene surface. Mechanical properties for pure graphene scrolls (fibers) are less impressive, 2.2 GPa strength and 0.3 TPa modulus, but are still competitive with those of carbon fibers. Better control in sample preparation can further improve mechanical properties of pure graphene samples and composites. Reported electrical conductivities for laminates are 8.1 S/cm at only 0.13% graphene volumetric loadings and 5×10^3 S/cm for pure graphene fibers.

METHODS

Graphene Synthesis. Graphene was grown by CVD as described earlier.[20,21] In brief, electropolished copper foils (25 or 125 μm thick) were loaded into an atmospheric pressure CVD reactor and annealed at either 1010 °C (25 μm foil) or 1065 °C (125 μm foil). Foil annealing was done under a flow of 2.5% H_2 in Ar for 30 min. Graphene growth was performed by addition of methane with gradual increase of its concentration from 14 to 20, 40, and 100 ppm for 30 min in each step. After growth, Microchem PMMA 495A4 solution was spin-coated at 1500 rpm on top of graphene on copper foil. Graphene from the back side of copper was etched away by oxygen plasma, and the copper was dissolved by 1 M $FeCl_3$ in 3% HCl. The graphene/PMMA sandwich floating on the surface of water was washed by DI water and transferred on the substrate of interest. As was shown before,[20,21] such a procedure leads to a high-quality graphene with domain size in excess of 100 μm and less than 5% of second-layer coverage.

Graphene Volumetric Loading. Graphene loading of 0.13% was calculated using measured thickness and the number of graphene layers in the laminate according to eq S1. (See section IX, Supporting Information, for details.) The number of graphene layers was independently confirmed by UV−vis measurements (Figure 1c and description in the text).

Type-1 Sample Preparation. Graphene laminates were prepared by sequential transfer of Gr/PMMA sandwiches (grown on 25 μm thick foil) onto the top of the previous layer. Graphene grown on 125 μm thick copper foil served as the bottom substrate for all transfers because thicker foils are easier to handle. After each layer, the structure was allowed to dry for several hours and then annealed at 150 °C for 5 min on a hot plate. $(Gr/PMMA)_{16}$ was prepared from two $(Gr/PMMA)_8$ laminates annealed together. $(PMMA)_{16}$ was prepared in a similar way, with each PMMA layer spin-coated on an annealed copper foil without graphene.

DOI: 10.1021/acsami.5b01367
ACS Appl. Mater. Interfaces 2015, 7, 10702−10709

Type-2 Sample Preparation. $(Gr)_x/(PMMA)_1$ films were prepared in a way similar to that for type-1 samples, but after each sequential graphene/PMMA sandwich transfer and baking, PMMA was dissolved in acetone for 1 h, rinsed with IPA, and dried under air gun. The $(Gr)_x/(PMMA)_1$ structure released from copper, floating on top of DI water, was rolled onto a 0.7 mm diameter wire in a manner similar to the previously reported procedure of scroll preparations for fabrication of optical structures.[58] The wire surface was lubricated with Dow Corning high-vacuum silicone grease for easy $(Gr)_x/(PMMA)_1$ scroll removal from the wire. After rolling, the fiber/scroll was dried under ambient conditions overnight and carefully pulled from the wire. $(Gr)_6$ fiber was prepared by dissolving PMMA of $(Gr)_6(PMMA)_1$ fiber in acetone overnight. After PMMA dissolution, the fiber was transferred to IPA, soaked for several hours, and then dried on a paper tissue.

Measurements. Type-1 samples were mounted either on a homemade setup (Supporting Information) or a Linkam Instruments TST350 stage with a 20 N load cell. Mounting was performed using double-sided Scotch tape in the following order: Scotch tape was put on the stage clamps first, followed by having the sample being carefully pressed onto the Scotch tape, and finally, another tape was added on top of the laminate. All samples broke in the middle of the gauge section, as Figure 2 shows, indicating that the process for transferring load to the test specimen did not influence the failure process. Type-2 samples were measured on an MTS Alliance RT/5 instrument with a 5 N load cell. Mounting was typically performed with double-sided Scotch tape in a manner similar to that used with type1 samples. $(Gr)_6$ samples were mounted by either double-sided Scotch or superglue without a noticeable difference in these two approaches. Type-2 samples had a tendency to break close to the mounting point, but the presented data are only for fibers that broke at least 2 mm away from the mounting point. Displacement rates for measurements with type-1 samples were 0.4 mm/min (initial strain rate = 4%/min) and 0.1 mm/min for measurements with type-2 samples (initial strain rate ≈ 0.5−1%/min). Typical gauge length was 1 cm for both sample types. E_E, σ_E, E_{PMMA}, and σ_{PMMA} values were derived from at least three independent stress−strain measurements. Ultimate strength (σ_E and σ_{PMMA}) was calculated from maximum stress that the sample had to withstand before fracture. E_E and E_{PMMA} were calculated on the initial linear part (up to 1% strain) of the stress−strain curves. For the electrical conductivity measurements and LED suspension, fibers or laminates were mounted by conductive epoxy. The electrical resistance was measured in a two-point scheme, and the conductivity was calculated from sample dimensions (Supporting Information).

■ ASSOCIATED CONTENT

Supporting Information

Optical/SEM characterization; stress-modulus chart; strain−stress curves of graphene fibers; laminate thickness measurements; GIWAXS, DSC, and conductivity measurements; data and error analysis. The Supporting Information is available free of charge on the ACS Publications website at DOI: 10.1021/acsami.5b01367.

■ AUTHOR INFORMATION

Corresponding Author

*E-mail: vlassioukiv@ornl.gov.

Notes

The authors declare no competing financial interest.

■ ACKNOWLEDGMENTS

We thank Xiong Fue and Hippolyte Grappe for assistance with strain−stress measurements of type-2 samples. This research was supported by the Laboratory Directed Research and Development Program of ORNL, managed by UT-Battelle, LLC, for the U.S. Department of Energy. A portion of this research was conducted at the Center for Nanophase Materials Sciences, which is sponsored at Oak Ridge National Laboratory by the Scientific User Facilities Division, U.S. Department of Energy. The Oak Ridge National Laboratory is operated for the U.S. Department of Energy by UT-Battelle under contract no. DE-AC05-00OR22725.

■ REFERENCES

(1) Lee, C.; Wei, X.; Kysar, J.; Hone, J. Measurement of the Elastic Properties and Intrinsic Strength of Monolayer Graphene. *Science* **2008**, *321*, 385−388.
(2) Young, R. J.; Kinloch, I. A.; Gonga, L.; Novoselov, K. S. The Mechanics of Graphene Nanocomposites: A review. *Compos. Sci. Technol.* **2012**, *72*, 1459−1476.
(3) Hwang, S. H.; Kang, D.; Ruoff, R. S.; Shin, H. S.; Park, Y.-B. Poly(vinyl alcohol) Reinforced and Toughened with Poly(dopamine)-Treated Graphene Oxide, and Its Use for Humidity Sensing. *ACS Nano* **2014**, *8*, 6739−6747.
(4) Yooness, M.; Shi, Y.; Scheiman, D. A.; Lebron-Colon, M.; Tigelaar, D. M.; Weiss, R. A.; Meador, M. A. Graphene Polyimide Nanocomposites;Thermal, Mechanical, and High-Temperature Shape Memory Effects. *ACS Nano* **2012**, *6*, 7644−7655.
(5) Walker, L. S.; Marotto, V. R.; Rafiee, M. A.; Koratkar, N.; Corral, E. L. Toughening in Graphene Ceramic Composites. *ACS Nano* **2011**, *5*, 3182−3190.
(6) Khan, U.; May, P.; Porwal, H.; Nawaz, K.; Coleman, J. N. Improved Adhesive Strength and Toughness of Polyvinyl Acetate Glue on Addition of Small Quantities of Graphene. *ACS Appl. Mater. Interfaces* **2010**, *2*, 1707−1713.
(7) Yang, X.; Tu, Y.; Li, L.; Shang, S.; Tao, X.-M. Well-Dispersed Chitosan/Graphene Oxide Nanocomposites. *ACS Appl. Mater. Interfaces* **2013**, *5*, 1423−1428.
(8) Yang, C.; Li, L.; Shang, S.; Tao, X. Synthesis and Characterization of Layer-aligned Poly(vinyl alcohol)/Graphene Nanocomposites. *Polymer* **2010**, *51*, 3431−3435.
(9) Hu, K.; Kulkarni, D. D.; Choi, I.; Tsukruk, V. V. Graphene-Polymer Nanocomposites for Structural and Functional Applications. *Prog. Polym. Sci.* **2014**, *39*, 1934−1972.
(10) Hu, K.; Gupta, M. K.; Kulkarni, D. D.; Tsukruk, V. V. Ultra-Robust Graphene Oxide-Silk Fibroin Nanocomposite Membranes. *Adv. Mater.* **2013**, *25*, 2301−2307.
(11) Hu, K.; Tolentino, L. S.; Kulkarni, D. D.; Ye, C.; Kumar, S.; Tsukruk, V. V. Written-in Conductive Patterns on Robust Graphene Oxide Biopaper by Electrochemical Microstamping. *Angew. Chem.* **2013**, *52*, 13784.
(12) Paul, D. R.; Robeson, L. M. Polymer Nanotechnology: Nanocomposites. *Polymer* **2008**, *49*, 3187−3204 and references therein.
(13) Zeng, Q. H.; Yu, A. B.; Lu, G. Q.; Paul, D. R. Clay-Based Polymer Nanocomposites: Research and Commercial Development. *J. Nanosci. Nanotechnol.* **2005**, *5*, 1574−1592 and references therein.
(14) Koziol, K.; Vilatela, J.; Moisala, A.; Motta, M.; Cunniff, P.; Sennett, M.; Windle, A. High-Performance Carbon Nanotube Fiber. *Science* **2007**, *318*, 1892−1895.
(15) Behabtu, N.; Young, C. C.; Tsentalovich, D. E.; Kleinerman, O.; Wang, X.; Ma, A. W. K.; Bengio, E. A.; ter Waarbeek, R. F.; de Jong, J. J.; Hoogerwerf, R. E.; Fairchild, S. B.; Ferguson, J. B.; Maruyama, B.; Kono, K.; Talmon, Y.; Cohen, Y.; Otto, M. J.; Pasquali, M. Strong,

DOI: 10.1021/acsami.5b01367
ACS Appl. Mater. Interfaces 2015, 7, 10702−10709

Light, Multifunctional Fibers of Carbon Nanotubes with Ultrahigh Conductivity. *Science* **2013**, *339*, 182−186.
(16) Lu, W.; Zu, M.; Byun, J.-H.; Kim, B.-S.; Chou, T.-W. State of the Art of Carbon Nanotube Fibers: Opportunities and Challenges. *Adv. Mater.* **2012**, *24*, 1805−1833.
(17) Dikin, D. A.; Stankovich, S.; Zimney, E. J.; Piner, R. D.; Dommett, G. H. B.; Evmenenko, G.; Nguyen, S. T.; Ruoff, R. S. Preparation and Characterization of Graphene Oxide Paper. *Nature* **2007**, *448*, 457−460.
(18) Zhang, M.; Huang, L.; Chen, J.; Li, C.; Shi, G. Ultratough, Ultrastrong, and Highly Conductive Graphene Films with Arbitrary Sizes. *Adv. Mater.* **2014**, *26*, 7588−7592.
(19) Li, Z.; Young, R. J.; Kinloch, I. A. Interfacial Stress Transfer in Graphene Oxide Nanocomposites. *ACS Appl. Mater. Interfaces* **2013**, *5*, 456−463.
(20) Vlassiouk, I.; Smirnov, S.; Regmi, M.; Surwade, S. P.; Srivastava, N.; Feenstra, R.; Eres, G.; Parish, C.; Lavrik, N.; Datskos, P.; Dai, S.; Fulvio, P. Graphene Nucleation Density on Copper: Fundamental Role of Background Pressure. *J. Phys. Chem. C* **2013**, *117*, 18919−18926.
(21) Vlassiouk, I.; Fulvio, P.; Meyer, H.; Lavrik, N.; Dai, S.; Datskos, P.; Smirnov, S. Large Scale Atmospheric Pressure Chemical Vapor Deposition of Graphene. *Carbon* **2013**, *54*, 58−67.
(22) Kim, Y.; Lee, J.; Yeom, M. S.; Shin, J. W.; Kim, H.; Cui, Y.; Kysar, J. W.; Hone, J.; Jung, Y.; Jeon, S.; Han, S. M. Strengthening Effect of Single-Atomic-Layer Graphene in Metal−Graphene Nanolayered Composites. *Nat. Commun.* **2012**, *4*, 2114.
(23) Podsiadlo, P.; Kaushik, A. K.; Arruda, E. M.; Waas, A. M.; Shim, B. S.; Xu, J.; Nandivada, H.; Pumplin, B. G.; Lahann, J.; Ramamoorthy, A.; Kotov, N. A. Ultrastrong and Stiff Layered Polymer Nanocomposites. *Science* **2007**, *318*, 80−83.
(24) Shim, B. S.; Tang, Z.; Morabito, M. P.; Agarwal, A.; Hong, H.; Kotov, N. A. Integration of Conductivity, Transparency, and Mechanical Strength into Highly Homogeneous Layer-by-Layer Composites of Single-Walled Carbon Nanotubes for Optoelectronics. *Chem. Mater.* **2007**, *19*, 5467−5474.
(25) Olek, M.; Ostrander, J.; Jurga, S.; Möhwald, H.; Kotov, N.; Kempa, K.; Giersig, M. Layer-by-Layer Assembled Composites from Multiwall Carbon Nanotubes with Different Morphologies. *Nano Lett.* **2004**, *4*, 1889−1895.
(26) Li, X.; Warzywoda, J.; McKenna, G. B. Mechanical Responses of a Polymer Graphene-Sheet Nano-Sandwich. *Polymer* **2014**, *55*, 4976−4982.
(27) Lee, G.-H.; Cooper, R. C.; An, S. J.; Lee, S.; van der Zande, A.; Petrone, N.; Hammerberg, A. G.; Lee, C.; Crawford, B.; Oliver, W.; Kysar, J. W.; Hone, J. High-Strength Chemical Vapor−Deposited Graphene and Grain Boundaries. *Science* **2013**, *340*, 1073−1076.
(28) Rasool, H. I.; Ophus, C.; Klug, W. S.; Zettl, A.; Gimzewski, J. K. Measurement of the Intrinsic Strength of Crystalline and Polycrystalline Graphene. *Nat. Commun.* **2013**, *4*, 2811.
(29) Song, Z.; Artyukhov, V. I.; Yakobson, B. I.; Xu, X. Pseudo Hall−Petch Strength Reduction in Polycrystalline Graphene. *Nano Lett.* **2013**, *13*, 1829−1833.
(30) Grantab, R.; Shenoy, V. B.; Ruoff, R. S. Anomalous Strength Characteristics of Tilt Grain Boundaries in Graphene. *Science* **2013**, *330*, 946−948.
(31) Zandiatashbar, A.; Lee, G. H.; An, S. J.; Lee, S.; Mathew, N.; Terrones, M.; Hayashi, T.; Picu, C. R.; Hone, J.; Koratkar, N. Effect of Defects on the Intrinsic Strength and Stiffness of Graphene. *Nat. Commun.* **2014**, *5*, 3186.
(32) Zhang, P.; Ma, L.; Fan, F.; Zeng, Z.; Peng, C.; Loya, P. E.; Liu, Z.; Gong, Y.; Zhang, J.; Zhang, X.; Ajayan, P. M.; Zhu, T.; Lou, J. Fracture Toughness of Graphene. *Nat. Commun.* **2014**, *5*, 3782.
(33) Lee, J.-U.; Yoon, D.; Cheong, H. Estimation of Young's Modulus of Graphene by Raman Spectroscopy. *Nano Lett.* **2012**, *12*, 4444−4448.
(34) Wang, H.; Keum, J. K.; Hiltner, A.; Baer, E.; Freeman, B.; Rozanski, A.; Galeski, A. Confined Crystallization of Polyethylene Oxide in Nanolayer Assemblies. *Science* **2009**, *323*, 757−760.
(35) Carra, J. M.; Langhea, D. S.; Pontinga, M. T.; Hiltnera, A.; Baera, E. Confined Crystallization in Polymer Nanolayered Films: A review. *J. Mater. Res.* **2012**, *27*, 1326−1350.
(36) Stafford, C. M.; Vogt, B. D.; Harrison, C.; Julthongpiput, D.; Huang, R. Elastic Moduli of Ultrathin Amorphous Polymer Films. *Macromolecules* **2006**, *39*, 5095−5099.
(37) Frank, O.; Tsoukleri, G.; Riaz, I.; Papagelis, K.; Parthenios, J.; Ferrari, A. C.; Geim, A. K.; Novoselov, K. S.; Galiotis, C. Development of a Universal Stress Sensor for Graphene and Carbon Fibres. *Nat. Commun.* **2011**, *2*, 255.
(38) Yu, T.; Ni, Z.; Du, C.; You, Y.; Wang, Y.; Shen, Z. Raman Mapping Investigation of Graphene on Transparent Flexible Substrate: The Strain Effect. *J. Phys. Chem. C* **2008**, *112*, 12602−12605.
(39) Mohiuddin, T. M. G.; Lombardo, A.; Nair, R. R.; Bonetti, A.; Savini, G.; Jalil, R.; Bonini, N.; Basko, D. M.; Galiotis, C.; Marzari, N.; Novoselov, K. S.; Geim, A. K.; Ferrari, A. C. Uniaxial Strain in Graphene by Raman Spectroscopy: G Peak Splitting, Grüneisen Parameters, and Sample Orientation. *Phys. Rev. B* **2009**, *79*, 205433.
(40) Ni, Z. H.; Yu, T.; Lu, Y. H.; Wang, Y. Y.; Feng, Y. P.; Shen, Z. X. Uniaxial Strain on Graphene: Raman Spectroscopy Study and Band-Gap Opening. *ACS Nano* **2008**, *2*, 2301−2305.
(41) Huanga, M.; Yan, H.; Chen, C.; Song, D.; Heinz, T. F.; Hone, J. Phonon Softening and Crystallographic Orientation of Strained Graphene Studied by Raman Spectroscopy. *Proc. Nat. Acad. Sci. U.S.A.* **2009**, *106*, 7304−7308.
(42) Gong, L.; Kinloch, I. A.; Young, R. J.; Riaz, I.; Jalil, R.; Novoselov, K. S. Interfacial Stress Transfer in a Graphene Monolayer Nanocomposite. *Adv. Mater.* **2010**, *22*, 2694−2697.
(43) Jiang, T.; Huang, R.; Zhu, Y. Interfacial Sliding and Buckling of Monolayer Graphene on a Stretchable Substrate. *Adv. Funct. Mater.* **2014**, *24*, 396−402.
(44) Calado, V. E.; Schneider, G. F.; Theulings, A. M. M. G.; Dekker, C.; Vandersypen, L. M. K. Formation and Control of Wrinkles in Graphene by the Wedging Transfer Method. *Appl. Phys. Lett.* **2012**, *101*, 103116.
(45) Li, Z.; Kinloch, I. A.; Young, R. J.; Novoselov, K. S.; Anagnostopoulos, G.; Parthenios, J.; Galiotis, C.; Papagelis, K.; Lu, C.-Y.; Britnell, L. Deformation of Wrinkled Graphene. *ACS Nano* **2015**, *9*, 3917−3925.
(46) Ericson, L. M.; Fan, H.; Peng, H.; Davis, V. A.; Zhou, W.; Sulpizio, J.; Wang, Y.; Booker, R.; Vavro, J.; Guthy, C.; Parra-Vasquez, A. N. G.; Kim, M. J.; Ramesh, S.; Saini, R. K.; Kittrell, C.; Lavin, G.; Schmidt, H.; Adams, W. W.; Billups, W. E.; Pasquali, M.; Hwang, W.-F.; Hauge, R. H.; Fischer, J. E.; Smalley, R. E. Macroscopic, Neat, Single-Walled Carbon Nanotube Fibers. *Science* **2004**, *305*, 1447−1450.
(47) Zhong, X.-H.; Li, Y. L.; Liu, Y.-K.; Qiao, X.-H.; Feng, Y.; Liang, J.; Jin, J.; Zhu, L.; Hou, F.; Li, J.-Y. Continuous Multilayered Carbon Nanotube Yarns. *Adv. Mater.* **2010**, *22*, 692−696.
(48) Wang, X.; Bai, H.; Yao, Z.; Liua, A.; Shi, G. Electrically Conductive and Mechanically Strong Biomimetic Chitosan/Reduced Graphene Oxide Composite Films. *J. Mater. Chem.* **2010**, *20*, 9031−9036.
(49) Pham, V. H.; Dang, T. T.; Hur, S. H.; Kim, E. J.; Chung, J. S. Highly Conductive Poly(methyl methacrylate) (PMMA)-Reduced Graphene Oxide Composite Prepared by Self-Assembly of PMMA Latex and Graphene Oxide through Electrostatic Interaction. *ACS Appl. Mater. Interfaces* **2012**, *4*, 2630−2636.
(50) Chen, M.; Tao, T.; Zhang, L.; Gao, W.; Li, C. Highly Conductive and Stretchable Polymer Composites Based on Graphene/MWCNT Network. *Chem. Commun.* **2013**, *49*, 1612−1614.
(51) Tkalya, E.; Ghislandi, M.; Alekseev, A.; Koning, C.; Loos, J. Latex-Based Concept for the Preparation of Graphene-Based Polymer Nanocomposites. *J. Mater. Chem.* **2010**, *20*, 3035−3039.
(52) Stankovich, S.; Dikin, D. A.; Dommett, G. H. B.; Kohlhaas, K. M.; Zimney, E. J.; Stach, E. A.; Piner, R. D.; Nguyen, S. T.; Ruoff, R. S. Graphene-Based Composite Materials. *Nature* **2010**, *442*, 282−286.
(53) Pham, V. H.; Cuong, T. V.; Dang, T. T.; Hur, S. H.; Kong, B.-S.; Kim, E. J.; Shin, E. W.; Chung, J. K. Superior Conductive Polystyrene

DOI: 10.1021/acsami.5b01367
ACS Appl. Mater. Interfaces 2015, 7, 10702−10709

– Chemically Converted Graphene Nanocomposite. *J. Mater. Chem.* **2011**, *21*, 11312–11316.
(54) Yoonessi, M.; Gaier, J. R. Highly Conductive Multifunctional Graphene Polycarbonate Nanocomposites. *ACS Nano* **2010**, *4*, 7211–7220.
(55) Zhang, H.-B.; Zheng, W.-G.; Yan, Q.; Yang, Y.; Wang, J.-W.; Lua, Z.-H.; Ji, G.-Y.; Yub, Z.-Z. Electrically Conductive Polyethylene Terephthalate/Graphene Nanocomposites Prepared by Melt Compounding. *Polymer* **2010**, *51*, 1191–1196.
(56) Vadukumpully, S.; Paul, J.; Mahanta, N.; Valiyaveettil, S. Flexible Conductive Graphene/Poly(vinyl chloride) Composite Thin Films with High Mechanical Strength and Thermal Stability. *Carbon* **2011**, *49*, 198–205.
(57) Steurer, P.; Wissert, R.; Thomann, R.; Mülhaupt, R. Functionalized Graphenes and Thermoplastic Nanocomposites Based upon Expanded Graphite Oxide. *Macromol. Rapid Commun.* **2009**, *30*, 316–327.
(58) Kolle, M.; Lethbridge, A.; Kreysing, M.; Baumberg, J. J.; Aizenberg, J.; Vukusic, P. Bio-Inspired Band-Gap Tunable Elastic Optical Multilayer Fibers. *Adv. Mater.* **2013**, *25*, 2239–2245 and references therein.

DOI: 10.1021/acsami.5b01367
ACS Appl. Mater. Interfaces 2015, 7, 10702–10709